Investigating the effect of grain structure on compressive response of open-cell metal foam using high-fidelity crystal-plasticity modeling

Dongfang Zhao [a], Kristoffer E. Matheson [a], Brian R. Phung [a], Steve Petruzza [b,c], Michael W. Czabaj [a], Ashley D. Spear [a,*]

[a] *Department of Mechanical Engineering, University of Utah, Salt Lake City, UT, USA*
[b] *Scientific Computing and Imaging Institute, University of Utah, Salt Lake City, UT, USA*
[c] *Department of Computer Science, Utah State University, Logan, UT, USA*

ARTICLE INFO

ABSTRACT

The mechanical response of open-cell metallic foams depends strongly on their hierarchical structure, which ranges from the grain scale, to the scale of individual struts, to the scale of the bulk foam. The objective of this study is to investigate the effect of grain structure on the compressive mechanical response of open-cell metallic foam using a crystal-plasticity finite-element-based framework. Multiple polycrystalline instantiations (overlaid on a foam volume derived from X-ray tomography) are simulated to quantify the grain-size effect on crushing response of investment-cast aluminum foam. The high-fidelity numerical framework captures the deformation mechanisms across multiple length scales and is able to predict the inhomogeneous grain-to-continuum compressive response in the foams. Also, by incorporating grain-boundary strengthening and free-surface softening mechanisms, the current framework accounts simultaneously for the Hall-Petch effect in polycrystalline alloys and the effect of unconstrained slip-based deformation at the strut free surfaces. The crystal-plasticity simulations explicitly account for the effect of grain structure and surface conditions (oxidized or non-oxidized) and provide new insights into the mechanical behavior of open-cell metallic foams. Results show that the relationship between grain size and plateau stress in the foams follows a Hall-Petch-like trend provided there is at least one complete grain along the strut length and approximately one grain through the strut thickness; below this threshold, the effective plateau stress of the foam tends to saturate. In the presence of an oxidation layer, when the dislocations are blocked at the strut boundaries, the effect of grain structure on plateau stress is less pronounced than when an oxidation layer is absent. It is also shown that by accounting for grain size and surface condition through the parameters σ_y and C_4, the accuracy and generalizability of the well-established Gibson-Ashby model for plastic collapse strength can be significantly enhanced.

1. Introduction

Open-cell metallic foams are hierarchical structural-material systems that comprise the component scale of the engineered part, the topological scale of interconnected ligaments (or struts), and the grain scale within individual ligaments. The relative density of open-cell foams can be as low as 0.01 [1], and their structural topology can range from stochastic polyhedral cells to highly ordered lattice structures, which are becoming increasingly common thanks to additive manufacturing. These cellular structural materials have potential multi-functional applications due to their low-density and hierarchical structure [2–4]. For example, in addition to serving as light-weight, load-bearing structures,

open-cell metallic foams have potential applications as electrodes for energy-storage devices [5], as hosts for newly generated bone and blood vessels in biomedical implants [6–8], or as impact absorbers and noise insulators for advanced high-speed ground transportation [4].

There have been considerable efforts in the literature to study the topological-scale deformation mechanisms and the overall mechanical behavior of open-cell metal foam. Some of the efforts have characterized foam specimens with advanced experimental techniques [9–14]. For example, Jang et al. [9] investigated the dependence of cell size and cell anisotropy on the compressive responses of aluminum (Al-6101-T6) Duocel® foams. Schüler et al. [10] elucidated the role of hierarchical structural elements (e.g., foam cells, struts, and strut microstructures) on

---

* Corresponding author.
E-mail address: ashley.spear@utah.edu (A.D. Spear).

the macroscopic deformation and failure behavior under quasi-static and dynamic loading conditions. The localized deformation in the locally weakened struts destabilized the adjacent cells and the interconnected struts. This caused the formation of macroscopic deformation bands and the apparent plateau region in global stress-strain curve. They also found that the intermetallic phases (Si, Mg_2Si, AlSiFe) inherent to the struts resulted in a more brittle behavior, while the Al-matrix (α phase) enhanced the ductility of the struts. Additionally, Kaya et al. [12] attributed the strut deformation mechanisms to their initial defects, micro-porosity, and strut orientation relative to the loading axis in powder-metallurgical manufactured stainless-steel foams. In that work, the struts deformed in bending and torsion to form plastic hinges when they were aligned perpendicular to the loading direction; while the struts buckled and initiated cracks as they were oriented parallel to the loading direction.

Modeling efforts in the literature have represented open-cell metal foams using either fully synthetic geometries or by reconstructing foam volumes from real measured data, for example, from X-ray computed tomography (CT). Subsequently, virtual tests have been performed on the three-dimensional (3D) open-cell foam models to enable prediction of their mechanical properties [15–22]. For example, the software, Surface Evolver, was used in the work by Gaitanaros et al. [15] to generate stochastic-foam models with realistic ligaments and anisotropic, randomly monodispersed cells. Frictional contact among ligaments and elasto-plastic material behavior of the Al-alloy were incorporated in the simulations to examine the effects of cellular randomness on the compressive responses in both longitudinal and transverse directions of the foam. Hangai et al. [19] created an analytical model of 3D aluminum foam based on X-ray CT images followed by finite-element analysis of the deformation behavior. They were able to predict the region where deformation first initiated under compressive loading and validated the numerical results with experiment. It was found that the deformation initiated in the plane that was perpendicular to the loading direction and contained a local maximum value of mean stress. Jang et al. [17] modeled open-cell foam structure with anisotropic, periodically dispersed Kelvin cells and realistic ligament geometries established by X-ray CT. The mechanical properties predicted by the numerical framework were compared with experimental data to evaluate the accuracy of the framework. Additionally, the work of Brydon et al. [21] and Bardenhagen et al. [20] demonstrated the capability of simulating complex contact mechanics and large-scale foam deformations in the densification regime via the material point method (MPM). While these studies provide critical insights into the topological-scale deformation mechanisms via modeling a 3D open-cell foam, the deformation mechanisms across multiple length scales, accounting for the influence of the grain structure, have not to our knowledge been modeled.

Although the majority of studies have characterized open-cell foams at the topological/morphological scale, treating each strut as a material continuum, there have been a limited number of experimental studies that have investigated the heterogeneous grain structure and its influence on the multiscale mechanical responses of such foams [23–27]. For example, Plumb et al. [27] recently measured and mapped the 3D grain structure of open-cell metallic foam using integrated techniques of X-ray CT and far-field high-energy X-ray diffraction microscopy (HEDM). Their results indicated relatively large grains with nearly one grain spanning an entire strut in some instances, suggesting that size effects due to grain structure could play a crucial role in the mechanical behavior of the foam. Similar findings in the work of Zhou et al. [23,24] suggested that a single strut can consist of a large grain across the strut thickness or can consist of bamboo-structured grains, depending on the heat treatment conditions. Goussery et al. [28] performed various heat treatments on open-cell nickel foam specimens to achieve different grain sizes. They found that the yield strength of non-oxidized, hollow-strut foam followed a Hall-Petch relationship as long as the grain size was smaller than the strut wall thickness. Krishna et al. [29] studied the

effect of heat treatment on the cell wall microstructures and on the resulting mechanical behavior of open-cell 6101 aluminum foams under free and constrained compression. They found that heat treating at the temperature that was well above the standard annealing temperature of 6101 alloy for a long period of time would lead to grain and precipitate coarsening. The decreases in inherent matrix strength and the cracks growing along the grain boundaries resulted in a drop in the strength of heat treated samples. The work of Lee et al. [30] investigated the strut size effects due to grain structure or other inhomogeneities on the ultimate tensile strength of open-cell electrodeposited nickel foams. Additionally, some researchers investigated the effect of various manufacturing processes on the strength, ductility, or energy absorption of open-cell aluminum foam (e.g., see Refs. [31–36]), attributing the variations in macroscopic behavior to the microscopic features of the struts including the arrangement and size of precipitates and the morphology of intermetallic phases. While the above experimental studies suggest that the grain structure could play a crucial role in determining the mechanical response of open-cell foam, such findings have yet to be incorporated into a numerical modeling framework to comprehensively investigate the effect of 3D grain structure on the multiscale mechanical response of open-cell metal foams or lattice structures.

The objective of this work is to elucidate and quantify the effect of grain size on the compressive response of open-cell aluminum foam, accounting for both the presence and absence of an oxidation layer on the free surfaces of the foam. To achieve this objective, a high-fidelity numerical framework is implemented that resolves 3D grain structure within the struts of the open-cell foam and leverages a crystal-plasticity constitutive model to account for plastic deformation due to crystallographic slip. The results provide new insight that can be used to inform the parameters in the well-known Gibson-Ashby model and to establish process-structure-property relationships to support performance-based design of open-cell metallic foams and lattice structures.

2. Material and methods

A crystal-plasticity finite-element modeling (CPFEM) framework used to investigate the grain-to-continuum compressive response of open-cell aluminum foam is introduced in this section. The modeled foam geometry is based on X-ray CT measurements, and the grain structure is instantiated by overlaying the CT reconstruction with synthetic yet realistic grains, thus producing a grain-resolved open-cell foam model. A grain-size parametric study is conducted by overlaying eight different grain structures on top of the same X-ray CT-imaged foam volume and simulating the crushing response in both the presence and absence of an oxidation layer on the free surfaces of the foam struts. These steps are detailed in the following subsections.

2.1. Generation of grain-resolved open-cell foam models

The material used in this study is an open-cell, investment-cast aluminum foam fabricated from a base aluminium alloy 6101 and strengthened with T6 heat treatment. The foam volume is reported to have a pore density of 40 pores per inch (PPI) and a relative density in the range of 6–8%. A cylindrical sample (10.1 mm in diameter and 12.7 mm in length) was machined out of the bulk foam using wire electrical discharge machining. The cylindrical sample comprised more than 10 cells per direction to avoid specimen size effects in global macroscopic mechanical response (i.e., the mechanical response of the sample is considered to be representative of the mechanical response of the bulk foam) [37]. The undeformed sample was imaged using a Varian BIR 150/130 X-ray CT imaging system (14 μm voxel spacing), producing a stack of 16-bit grayscale tomographic images. The tomographic images were segmented and virtually reconstructed in Avizo®, resulting in an STL file depicting the 3D foam morphology.

Because experimental characterization of 3D grain structure in ultra-

low-density foams is non-trivial [27], realistic synthetic grain structures are instantiated on the open-cell foam geometry using DREAM.3D [38]. DREAM.3D is an open-source software for digitally instantiating 3D, multi-phase microstructures based on directly or indirectly measured grain-scale statistics of interest (e.g., mean grain size, crystallographic orientation, grain morphology). Recently, Tucker and Spear [39] implemented an open-source filter in DREAM.3D to instantiate grain-resolved open-cell metal foam models. The new filter allows both for mapping physically realized grain structure on an existing foam morphology using measured statistics and for instantiating fully synthetic open-cell foam at both topological and grain scale. In the current study, the high-level workflow for instantiating grain-resolved open-cell foam models using DREAM.3D (v6.5.49) [39] is demonstrated in Fig. 1. In the first step (Fig. 1 (a)), a fully dense, polycrystalline domain is initialized with assigned dimensions, resolution, and origin. Crystal structure and goal grain statistics (e.g., size, shape, and crystallographic texture) are input and used to generate a statistically similar, fully dense, microstructural volume. In the second step, a foam mask (Fig. 1(b)) based on the X-ray CT data is applied to differentiate the voxels belonging to foam from the voxels belonging to the void space. Then, the voids in the polycrystalline domain are removed to reveal a grain-resolved open-cell foam model, as shown in Fig. 1(c). Note that although the current study uses equiaxed grains by specifying a spherical grain-growth (packing) algorithm, the general DREAM.3D workflow allows for modeling non-equiaxed grains. Grain metrics[1] are recorded for each grain in the foam volume, including the semi-axis lengths, aspect ratio, volume, and crystallographic orientation. Finally, a 3D hexahedral mesh is generated on the grain-resolved foam to enable subsequent numerical analysis. Readers can reference [38,39] for a detailed description of the DREAM.3D synthetic-microstructure generation process.

2.2. Slip-system-level constitutive model

To accurately predict the local, grain-scale mechanical deformation associated with crystallographic slip in polycrystalline materials, a crystal elasto-viscoplastic constitutive model has been implemented as a user material subroutine (VUMAT) into the commercial finite-element code ABAQUS® [40]. The CPFEM-based framework is demonstrated to be able to predict the inhomogeneous stresses and strains that evolve within polycrystalline materials and to quantify the interactions among discrete grains of different crystallographic orientations at the meso-scale. A number of studies have utilized the same crystal-plastic constitutive model (implemented with other solvers) to investigate the anisotropic, elasto-viscoplastic behavior in polycrystalline materials [41–45]. Readers can reference the work of Matouš and Maniatty [46] for a detailed description of the model formulation. A brief description is provided next for completeness.

In this study, crystallographic slip on the twelve octahedral slip systems {111}<110> of face-centered-cubic (fcc) crystals is assumed to be the only mechanism accounting for visco-plastic deformation. The constitutive model uses a multiplicative decomposition of the deformation gradient into an elastic part and a visco-plastic part:

$$F = F_e F_p. \tag{1}$$

The elastic Green-Lagrange strain tensor is given by

$$E_e = \frac{1}{2}\left(F_e^T F_e - I\right). \tag{2}$$

Behavior in the elastic regime assumes negligible thermal effects and a linear relationship with small elastic strain. The elastic stress-strain constitutive relation is summarized as:

$$S = \zeta : E_e, \tag{3}$$

where ζ denotes the fourth-order elasticity tensor. The second Piola-Kirchoff stress tensor, S, can be used to derive the Cauchy stress tensor, σ, based on the elastic deformation gradient, F_e:

$$\sigma = F_e\left(\frac{1}{det(F_e)}S\right)F_e^T. \tag{4}$$

Plastic deformation, which is accommodated by crystallographic slip, can be described by the slip rate on each slip system. The slip rate on slip system α is denoted $\dot{\gamma}^\alpha$ and is expressed as:

$$\dot{\gamma}^\alpha = \dot{\gamma}_0 \frac{\tau^\alpha}{g^\alpha}\left|\frac{\tau^\alpha}{g^\alpha}\right|^{\frac{1}{m}-1}, \tag{5}$$

where $\dot{\gamma}_0$ is a reference slip rate parameter, m is a material parameter describing the rate sensitivity, τ^α is the resolved shear stress on slip system α, and g^α is the resistance to crystallographic slip (critical resolved shear stress) for slip system α. The plastic velocity gradient, $\hat{L}_p$, is described in terms of the slip rate $\dot{\gamma}^\alpha$ as:

$$\hat{L}_p = \dot{F}_p F_p^{-1} = \sum_{\alpha=1}^{N_{ss}} \dot{\gamma}^\alpha P^\alpha, \tag{6}$$

where N_{ss} denotes the number of slip systems, and $P^\alpha = s^\alpha \otimes m^\alpha$ is the grain-orientation-related Schmid tensor, with s^α and m^α representing the slip direction and the slip plane normal for slip system α, respectively. Taking as input the crystal orientation of a given grain, the constitutive model then calculates the resolved shear stress in terms of the elastic deformation gradient and second Piola-Kirchoff stress tensor as:

$$\tau^\alpha = \left(F_e^T F_e S\right) : P^\alpha. \tag{7}$$

In the current work, a simplified version of the elasto-viscoplastic constitutive model is invoked, wherein hardening is neglected. The critical resolved shear stress, g^α, which is uniquely defined for every slip system and every element in the model (as described in the following subsection), is therefore held constant throughout the simulation. This simplification is justified for two reasons: (1) the main focus of the study is on the homogenized, large-scale crushing response of the foam, where localized hardening is assumed to be negligible compared to other structural mechanisms, like cell collapse, that govern the foam response; and (2) lack of grain-resolved mechanical test data precludes the ability to perform a more refined calibration than what we report in Section 2.4, which remains a topic of ongoing research by the authors.

2.3. Grain-boundary strengthening and free-surface softening mechanisms

In the original implementation of the above-mentioned constitutive model, grain-size effects were not explicitly accounted for. Thus, in this study, grain-boundary strengthening and free-surface softening mechanisms have been implemented into the CPFEM framework to account for, respectively, the Hall-Petch effect in polycrystalline materials and the effect of unconstrained slip-based deformation at free surfaces in the foam. In the current study, grain-boundary strengthening is incorporated by scaling the critical resolved shear stress, g^α, for each slip system of each element in the finite-element mesh. The scaled values of g^α are calculated prior to the CPFEM calculation based on the Euclidean distance directed along the specific slip direction to the nearest grain boundary, d_{GB}. In this manner, the slip-based directed-distance calculation accounts for the crystallographic orientation of each grain. The scaling relationship between the critical resolved shear stress and directed-distance to grain boundary for a given slip system and given element is calculated as:

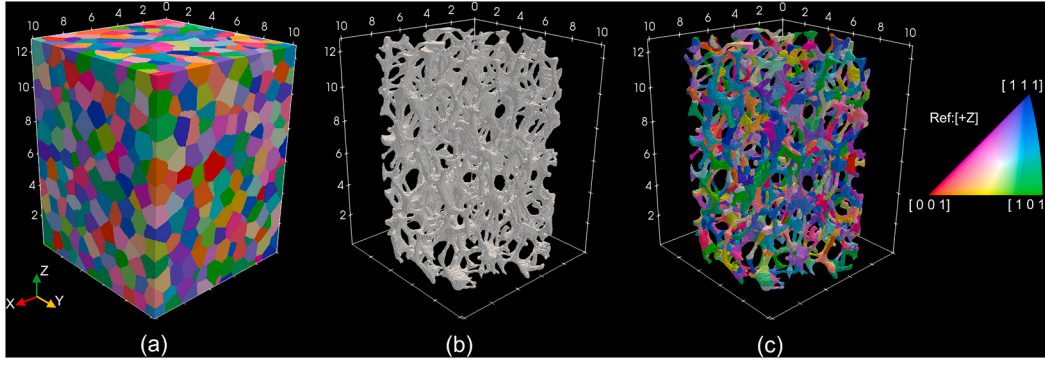[1] Geometrical metrics of each grain are based on best-fit ellipsoids.

Fig. 1. Process for generating grain-resolved open-cell foam models. (a) Synthetic fully dense polycrystal instantiated using DREAM.3D. (b) A foam mask determined from reconstruction of X-ray CT data. (c) Grain-resolved open-cell foam model generated by overlaying the foam mask with the polycrystalline domain. Inverse pole figure (IPF) map plotted with respect to the global z direction. Dimensions are in millimeters.

$$g^\alpha = g_\infty + \frac{\lambda_{GB}}{d_{GB}}, \tag{8}$$

where g_∞ represents the critical resolved shear stress for a point that is infinitely far from a grain boundary and λ_{GB} is a material parameter that represents the strengthening rate with distance to grain boundary. The implementation of the grain-boundary strengthening mechanism is verified on a fully dense polycrystalline cube, shown in Fig. 2, which illustrates the expected Hall-Petch behavior along with the stress field for representative volume elements (RVEs) of different grain size. The plot illustrates both the local effects of grain-boundary strengthening as well as the global effects on yield strength. The fitted Hall-Petch equation in Fig. 2 can be expressed as:

$$\sigma_y = 166.2 + \frac{198.2}{\sqrt{d}}, \tag{9}$$

where d is the average grain size represented by equivalent spherical diameter (*ESD*), in μm. The resulting Hall-Petch constant (198.2 MPa$\sqrt{\mu\text{m}}$) is comparable to values estimated for a similar

Al–Mg–Si alloy in the work of Nakai et al. [47].

Because open-cell foam has a large surface-to-volume ratio, the material is expected to soften due to the unconstrained motion of dislocations across free surfaces in the absence of an oxidation layer. Many researchers have investigated the interactions of dislocations and free surfaces, serving to motivate how free-surface softening is modeled in this study. For example, the work of Crone et al. [48] indicates a lower critical resolved shear stress required for dislocations to bypass an array of voids with the existence of free surfaces on their boundaries. They explained that the attractive image forces between dislocations and free surfaces reduced the strengthening effects of voids compared with other impenetrable inclusions. Additionally, Goussery et al. [28] found that the yield strengths of non-oxidized, hollow-strut, open-cell nickel foams were linearly related to their grain size as long as the grain size was smaller than the strut wall thickness. A saturation in yield strength was observed when the grain sizes were on the same scale as the strut wall thickness, and the reason attributed to this behavior was that the dislocation loops can escape easily across the strut boundaries. Also, Lee et al. [49] developed a half-space Peierls-Nabarro (HSPN) model to investigate the interactions between dislocations and free surfaces. They found that the Peierls barrier stress of a screw dislocation at a free surface was 5%–15% lower than that in the interior of bulk materials, which indicated more active dislocation motion near the free surface.

Similarly to the scaling relationship defined in Eqn. (8) for grain-boundary strengthening, free-surface softening is modeled in this study by scaling the critical resolved shear stress, g^α, based on the Euclidean distance, directed along a given slip system, to the nearest free surface, d_{FS}. Thus, the coupled effects of grain-boundary strengthening and free-surface softening are modeled by scaling the critical resolved shear stress, g^α, as follows:

$$g^\alpha = \frac{d_{GB}}{d_{GB} + d_{FS}} f(d_{GB}) + \frac{d_{FS}}{d_{GB} + d_{FS}} f(d_{FS}), \tag{10}$$

where

$$f(d_{GB}) = g_\infty + \frac{\lambda_{GB}}{d_{GB}}, \tag{11}$$

and

$$f(d_{FS}) = g_\infty + \frac{d_{FS}}{\lambda_{FS}}. \tag{12}$$

The material parameter λ_{FS} specifies the softening rate with respect to distance to free surface. The scaling relationship expressed in Eqn. (10) guarantees that g^α is defined in a smooth and continuous manner over the simulation domain.

In summary, oxidized and non-oxidized foams are modeled by scaling g^α for each slip system and each element using Eqns. (8) and (10).
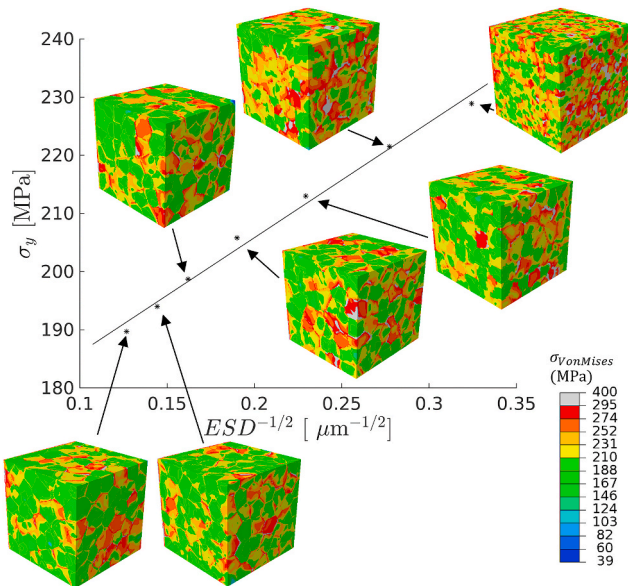

Fig. 2. Verification that updating g^α on each slip system according to Equation (8) approximately reproduces the macroscopic Hall-Petch behavior. Results of yield strength versus the inverse square root of grain size (based on equivalent spherical diameter) are shown for fully dense aluminum 6101-T6 with g_∞ and λ_{GB} values of 60.5 MPa and 60 MPa μm, respectively. The yield strength is determined at 0.2% offset strain line on the global stress-strain response.

In the former case, the oxidation layer is not explicitly modeled in the finite-element model; rather, the surfaces on the strut boundaries are implicitly modeled as barriers to dislocation motion by simply treating them as grain boundaries in the evaluation of Eqn. (8). In the latter case, Eqn. (10) is invoked only in grains that border strut boundaries and only for points within such grains that are closer to the strut free surface than to a grain boundary (along a specific slip direction); for all other elements within the model, including those within interior grains of a strut, g^α is scaled according to Eqn. (8). In terms of implementation for both oxidized and non-oxidized foam models, internal grain boundaries are distinguished from exterior strut boundaries based on unique identifiers assigned to different material regions (including void space) in the voxel-based representation described in Section 2.1.

2.4. Calibration of model parameters

The crystal-plasticity model parameters were calibrated by fitting the global force-displacement response of the modeled foam—resolved with realistic grain-structure—to the experimentally measured force-displacement response of the foam. The cylindrical volume of foam described in Section 2.1 was subjected to mechanical compression testing, and the resulting crush response was used to calibrate the CPFEM input parameters. The sample was uniaxially compressed under displacement control to a total displacement of 10.1 mm (79.5% of the initial height). The global mechanical response of the foam volume was plotted in terms of force versus displacement.

The undeformed foam sample reconstructed from X-ray CT imaging was then virtually overlaid with a realistic, synthetic grain structure (see Section 2.1) based on grain-scale measurements collected recently by Plumb et al. [27]. The results by Plumb et al. [27] suggest that the grains in a sample of investment-cast aluminum foam, similar to the sample described in Section 2.1, are of similar size to the strut length and that the grains are slightly elongated along strut lengths. The calibration model was thus overlaid with a grain structure that was similar to that of the foam measured by Plumb et al. [27]. Specifically, the mean grain *ESD* was targeted to be 0.45 mm with a target aspect ratio of 3.3:1.6:1. A total of 1033 grains was included in the calibration model. Crystal orientations of the grains in the calibration model were assigned to be uniformly random. The resulting distributions of grain-size metrics for the grain-resolved foam model used for calibration are plotted in Fig. 3.

The grain-resolved open-cell foam was then meshed and analyzed using ABAQUS Explicit [40] with the user subroutine described in Section 2.2. The model was meshed using linear hexahedral elements with reduced integration (C3D8R). To be consistent with the boundary conditions applied in experiment, the model was constrained between a top and bottom rigid plate, while all other sides remained unconstrained. The top rigid plate was displaced in the negative z-direction to approximately 40% crush strain, while all degrees of freedom on the bottom plate were fixed. Non-penetrable, frictional contact interactions were assigned among exterior surfaces of the foam and surfaces between

foam body and rigid plates with a coefficient of static friction for aluminum equal to 1.05 [50]. A mesh convergence study was conducted, and a nominal element size of 0.05 mm was found to provide sufficient convergence of the global force-displacement response, while maintaining computational tractability. The resulting finite-element model used for calibration comprised 564,844 linear hexahedral elements. A mass scaling study was also performed to improve computational efficiency and to ensure that inertial effects were negligible in the model, thereby replicating quasi-static loading.

The CPFEM constitutive-model input parameters were then iteratively adjusted until the simulated and experimental force-displacement responses matched. The model parameters controlling the shape of each region in the global force-displacement response were identified and adjusted to fit that respective region using a brute-force approach. Fig. 4 shows the global force-versus-displacement response of the calibration model, where the foam instantiation is colored by different grains. The calibrated material-model parameters are listed in Table 1. Note that the foam bulk and shear moduli (*K* and *G*, respectively) are lower than that in fully dense aluminum, which is consistent with the experimental observations in the work of Zhou et al. [23].

2.5. Parametric study of grain-size effects

The systematic study of grain-size effects on compressive response of open-cell aluminum foam is conducted by numerically overlaying the measured foam volume with different synthetic grain structures. A total of eight different grain-resolved open-cell foam instantiations are investigated in this study. To quantitatively analyze the statistics of the entire population of grains in each foam instantiation, a DREAM.3D pipeline is used that allows to represent each grain as a best-fit ellipsoid with the following parameters: aspect ratio (b/a, c/a), semi-axis length (a, b, c), and ellipsoidal volume. The *ESD* is then calculated from the given ellipsoidal volume. Based on the statistical distribution of grain metrics of each foam instantiation, the average (μ) and standard deviation (std dev) are calculated. The grain statistics of the eight grain-resolved open-cell foam models are shown in Fig. 5. The grain-resolved foam models range from having 23 grains to 20351 grains. The grain orientations for each foam instantiation are assigned to be uniformly random.

The same mesh type, finite-element solver, and boundary conditions as described in Section 2.4 are employed in the grain-size parametric study. Two separate studies are conducted to analyze the coupled effects of surface condition (oxidized versus non-oxidized) and grain structure on bulk mechanical response of open-cell aluminum foam. In the first case, the foam is considered to be non-oxidized, and a free-surface softening mechanism is invoked to emulate allowing the dislocations to escape across the free surfaces, as described by Eqn. (10). In the second case, the foam is considered to have an oxidation layer on the strut boundaries, and the free surfaces are treated as barriers to dislocation motion (analogous to grain boundaries), as described in Eqn. (8).
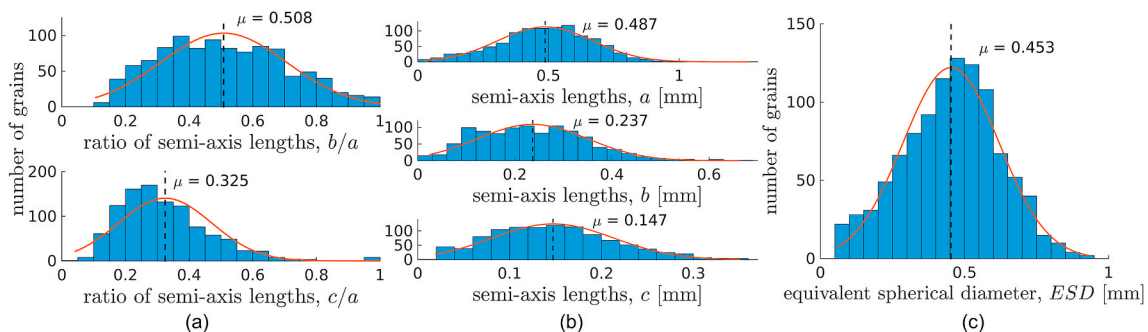

Fig. 3. Distributions of grain-size metrics in the grain-resolved foam model used for calibrating the crystal-plasticity model parameters. (a) aspect ratio, (b) semi-axis lengths, (c) equivalent spherical diameter.
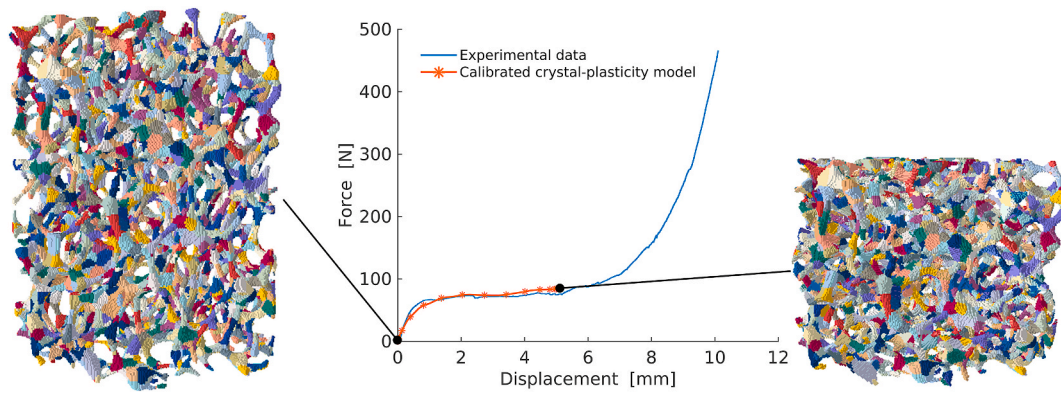
Fig. 4. Global force verse displacement response of the model used for crystal-plasticity model calibration. Simulations are performed to at least 40% crush strain to capture the plateau region of the response.

Table 1
Calibrated material-model parameters.

K	G	m	$\dot{\gamma}_0$	g_∞	$\lambda_{GB}, \lambda_{FS}$
18530 MPa	7105.3 MPa	0.0049	$1.0\,s^{-1}$	95.5 MPa	130 MPa·μm

In the subsequent results section, the global macroscopic force-displacement response is converted to effective stress ($\sigma_{eff} =$ force/ nominal undeformed cross-sectional area of the cylinder that encompasses the foam) versus effective compressive strain (δ/H) of the foam, where H is the initial height of the foam. Simulation up to 40% effective strain of the smallest-grain and largest-grain instantiations requires approximately 1696 core-hours and 1472 core-hours, respectively, on 32 cores within 2 Intel® Xeon® Gold 6130 CPU @ 2.10 GHz processors.

3. Results

3.1. Overview of grain-resolved foam instantiations

The grain structures within individual struts of all eight foam instantiations are shown in Fig. 6. In the small-grain instantiations (e.g., Fig. 6a, b and 6c), each strut has many interior, arbitrarily oriented grain boundaries. As the grain size increases from Fig. 6(a)–(h), the number of grain boundaries within a given strut decreases until there are few to no grain boundaries within a given strut (i.e., struts are spanned by entire crystals). Some of the grain structures depicted in Fig. 6 are qualitatively consistent with observations by Zhou et al. [23] based on microscale characterization of single struts from as-fabricated, annealed, and T6-strengthened aluminum 6101 foam. Note that in some of the large-grain instantiations modeled here (e.g., Fig. 6g and h), there are cases in which the average grain size is at least as large as the typical cell size of the foam. This is visually evident from several neighboring struts having the same crystal orientation (e.g., note instances of neighboring ligaments sharing the same IPF color in the large-grained instantiations depicted in Fig. 6). While it is possible to model such phenomena, it is unknown–due to the complexity of the solidification physics involved in investment casting of open-cell foams and the sparsity of grain-scale experimental data in the literature–whether such phenomena are physically possible or common. Because of the complexity of the solidification physics, the most current version of DREAM.3D used to the generate grain-resolved foam instantiations (v6.5.49) does not accommodate grain growth based on the solidification physics of investment casting, as mentioned in work by Tucker and Spear [39]. Future versions of the DREAM.3D plug-in could incorporate more realistic grain-growth algorithms, which is beyond the scope of this work. Nonetheless, the phenomenon of multiple neighboring struts having the same crystal orientation does not limit the applicability of the CPFEM modeling framework or the conclusions drawn in this study.

It is noted that very recent work by Wang et al. [51] demonstrated for the first time the capability of adaptively refining the grain size within open-cell Mg foams while keeping the strut-scale geometry constant by using a multi-axial forging process. The demonstrated ability to control grain size in physical samples of open-cell metallic foams bolsters the relevance and significance of the findings from this study.

3.2. Quantification of geometric features of the foam

Strut length and strut thickness were obtained for all struts within the foam volume using image analysis of the voxel-based model derived from X-ray CT. After stitching the X-ray CT images into a 3D volume, an isosurface representing the material boundaries was generated by applying a threshold on the 3D voxelized model and outputting a 3D PLY file, which can be directly visualized via the software ParaView [52]. The individual struts and nodes were identified using a combination of topological analysis techniques recently developed as part of a framework by Petruzza et al. [53]. In the framework, two different techniques are employed to extract nodes and struts. Nodes are segmented by computing a generalized geodesic density field, where high values identify points inside nodal structures. These segmented structures are later used to guide the identification of struts connecting nodes. More specifically, struts are extracted by computing the Morse-Smale complex [54] of the volume data and producing a 1-skeleton representation useful for extracting various properties, such as length and thickness (using cross sections along the 1-skeleton graph). Fig. 7 shows the distribution of strut length and thickness of the entire population of struts in the experimentally characterized foam volume depicted in Fig. 1(b). The average value of strut length (L) and strut thickness (t) is 1.43 mm and 0.27 mm, respectively.

3.3. Mechanical response of non-oxidized and oxidized foams

Figs. 8 and 9 show the effective stress-strain response of the bulk foam and its dependence on the underlying grain structure for the non-oxidized and oxidized conditions, respectively. Note that the vertical axis in Fig. 9 is truncated to match the scale of that in Fig. 8, enabling direct visual comparison between the two plots. Each curve is labeled according to the average number of grains along the strut length (L/2a) and average number of grains across the strut thickness (t/2c), where 2a and 2c are the average major- and minor-axis lengths based on a best-fit ellipsoid metric of grain size. All of the stress-strain curves have an initial linear-elastic region and exhibit the same compressive elastic modulus (approximately 19 MPa). Subsequently, the stress-strain responses deviate from one another, resulting in a grain-structure-sensitive plastic behavior. The onset of bulk yielding is followed by a region of relatively constant stress (stress plateau), which occurs just
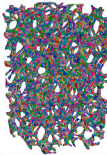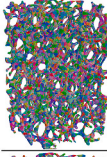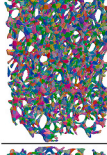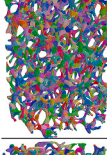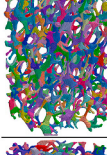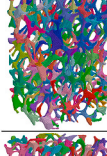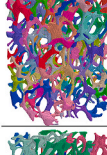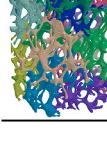
		Semi-axis length a [μm]	Semi-axis length b [μm]	Semi-axis length c [μm]	Aspect ratio b/a	Aspect ratio c/a	Equivalent spherical diameter ESD [μm]
	μ	131	88	62	0.68	0.49	169
	std dev	41	33	26	0.17	0.17	58
	μ	152	98	69	0.66	0.47	192
	std dev	52	39	30	0.17	0.17	71
	μ	188	117	82	0.63	0.44	230
	std dev	64	49	39	0.18	0.16	90
	μ	263	142	99	0.56	0.39	290
	std dev	95	63	47	0.19	0.15	115
	μ	487	237	147	0.51	0.33	450
	std dev	181	113	67	0.20	0.15	170
	μ	891	452	253	0.57	0.33	716
	std dev	241	167	99	0.18	0.14	206
	μ	980	587	351	0.61	0.36	890
	std dev	236	192	140	0.18	0.14	228
	μ	1833	1301	807	0.71	0.44	1710
	std dev	324	376	299	0.17	0.15	432

Fig. 5. Grain statistics of the eight grain-resolved open-cell foam instantiations.

before the onset of densification. The stress plateau, caused by buckling and localized plastic collapse of the struts, is characteristic of open-cell foams and contributes to the energy-absorption properties that make the foams attractive in specific applications.

In the case of the non-oxidized foam (Fig. 8), as the number of grains decreases along the strut length and across the strut thickness (i.e., as the grain size increases), the corresponding plateau stress decreases until an apparent threshold is reached. Below this threshold, which occurs when there is, on average, approximately one grain across the strut thickness and one complete grain along the strut length, the effective stress-strain response appears to saturate. The stress-strain responses of the oxidized foam (Fig. 9) are qualitatively similar to those without oxidation. However, the effect of grain structure is less pronounced in the case of oxidized foam than in non-oxidized foam, which is discussed further in

Section 4.1.

Figs. 10 and 11 present two important performance metrics extracted from the stress-strain curves for the non-oxidized and oxidized foams, respectively: plateau stress (also referred to as crush strength or plastic collapse strength) and energy absorption capacity. The plateau stress, $\sigma_{plateau}$, corresponds to a relatively constant value of σ_{eff} with respect to δ/H. The energy absorption capacity, U, is defined as the total area under the σ_{eff} versus δ/H curve, evaluated up to a predetermined level of effective strain (40% in this case). Outside of the threshold region described above, both $\sigma_{plateau}$ and U appear to increase approximately linearly with inverse square root of grain size (quantified in terms of ESD), which is analogous to typical Hall-Petch behavior observed in fully dense polycrystalline metals. Hence, Figs. 10 and 11 present $\sigma_{plateau}$ and U plotted with respect to $ESD^{-1/2}$ for all sixteen numerical
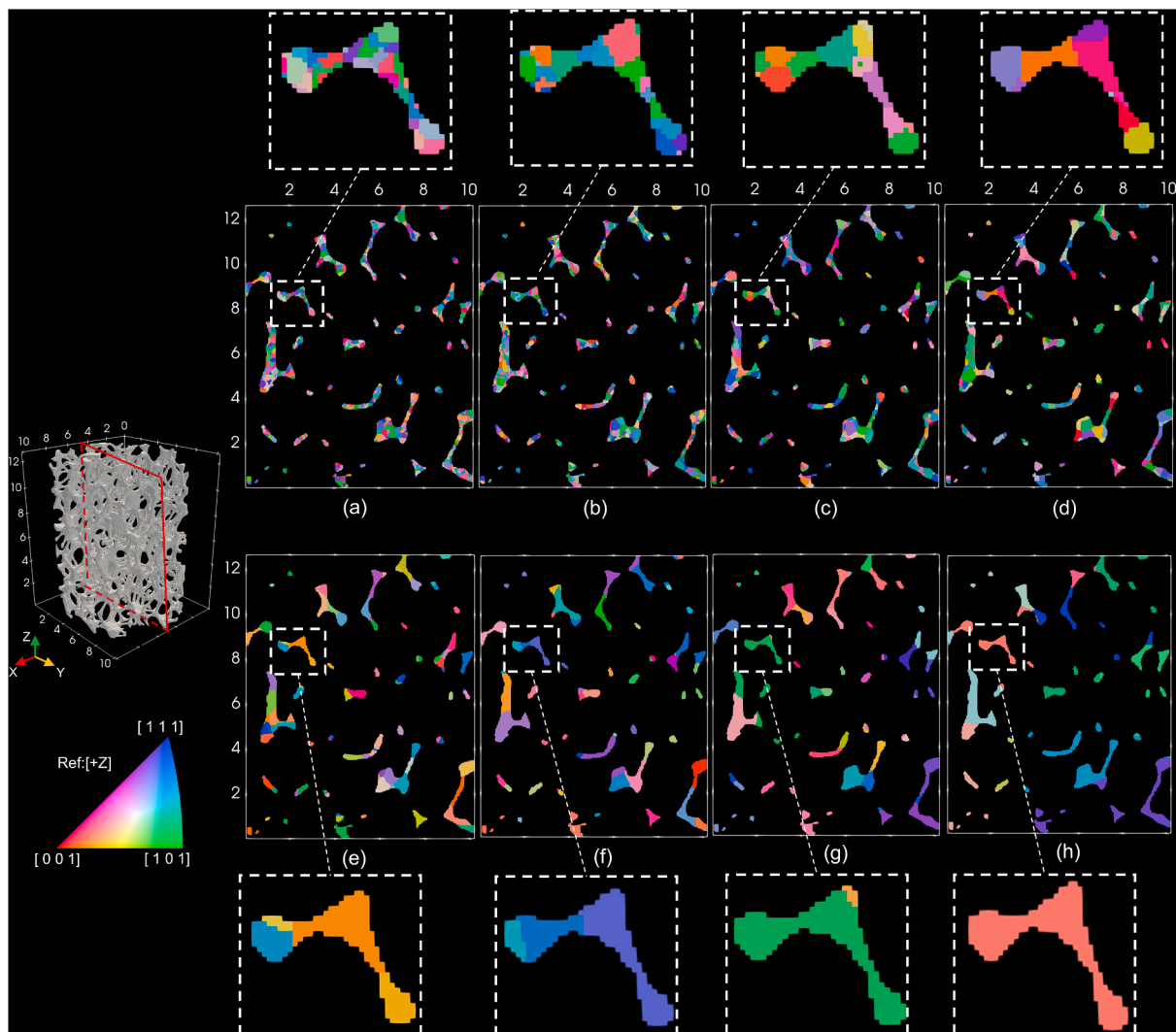
Fig. 6. A cross-sectional view of the open-cell foam depicting grain structure among the eight different instantiations. Images (a)–(h) correspond to the cross-section indicated on the 3D foam volume shown at left. For each instantiation, both oxidized and non-oxidized surface conditions were modeled. Colors represent crystal orientation using standard IPF mapping, plotted with respect to the z direction. Dimensions are in millimeters. (For interpretation of the references to color in this figure legend, the reader is referred to the Web version of this article.)

simulations. The Hall-Petch-like representations are plotted using two linear fits, one corresponding to data points that fall at or below the saturation threshold depicted in Fig. 8 and another corresponding to the remaining data points. As shown in Figs. 10 and 11, the slope of the linear fit through the three cases below saturation is very shallow or close to zero for both the plateau stress and energy absorption capacity. It is noted that a similar saturation phenomenon was observed for the experimentally measured yield strength of hollow-strut nickel foams studied by Goussery et al. [28]. Notably, similar to Goussery's observations and to recent observations by Wang et al. [51] on effect of grain size on open-cell Mg foams, the slope of the Hall-Petch-like curve for the foam ($k_{pl} = 0.183 \, \mathrm{MPa} \sqrt{\mathrm{mm}}$ in Fig. 10(a)) is found to be approximately two orders of magnitude smaller than that of the corresponding fully dense alloy.

While the plateau stress of the oxidized foam is 38%–65% greater than that of the corresponding non-oxidized foam for an equivalent grain structure, the range in plateau stress is much greater for the non-oxidized foam than the oxidized foam. The non-oxidized foam exhibits a 24% difference between the highest and lowest plateau stresses; whereas, the oxidized foam exhibits just a 6% difference. This observation is also apparent in the different slopes, k_{pl}, of the Hall-Petch-like curves (beyond the saturation region) presented in Figs. 10(a) and 11(a).

Similar trends are observed for the energy absorption capacity. These results are discussed further in the next section.

4. Discussion

4.1. Effect of grain size on mechanical response of oxidized and non-oxidized open-cell foams

The results presented in Section 3.3 provide insights into the coupled effects of surface conditions (non-oxidized versus oxidized) and grain structure on the mechanical response of open-cell metallic foam. For both surface conditions, there is an apparent saturation in the plateau stress and energy absorption capacity when there is nominally less than one complete grain along the strut length (i.e., when, on average, the grains extend beyond the length of the struts) and approximately one grain through the strut thickness. Once the grains are relatively large with respect to the strut size (i.e., generally no grain boundaries within most struts), the crushing response tends to saturate. A likely reason for this apparent saturation is that the mean free path for dislocation motion becomes limited by the geometrical constraints of the struts rather than by the grain boundaries, which is not the case for fully dense poly-crystalline metals. When the struts generally contain more than one
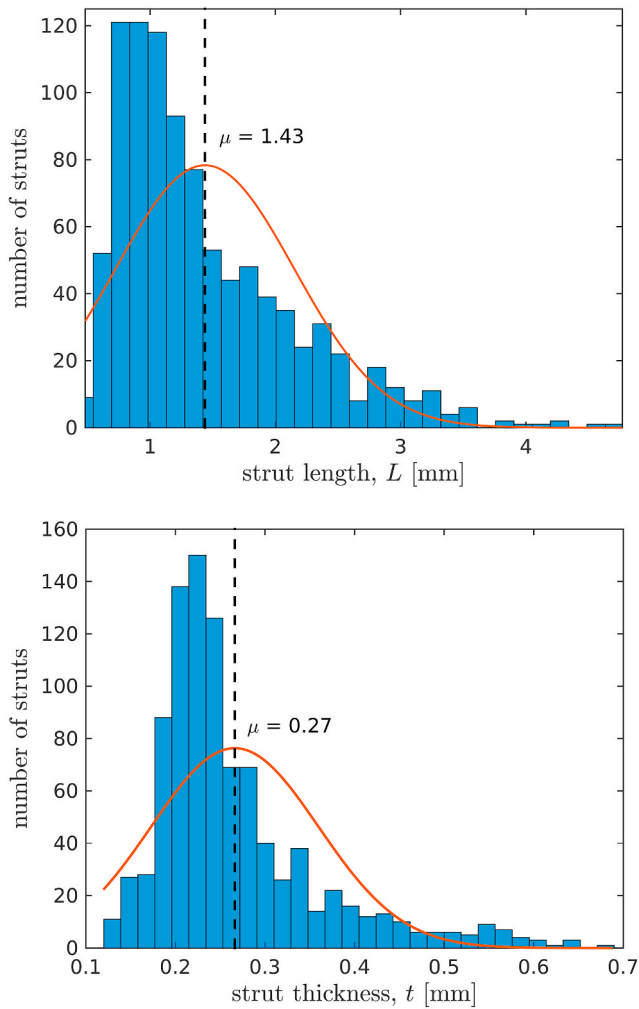
Fig. 7. Histogram of strut length and thickness for the entire population of struts in the experimentally characterized foam depicted in Fig. 1(b).

Fig. 8. Effective stress-strain responses of different grain-resolved, **non-oxidized** foam models. The average grain size is normalized by average geometric parameters of the struts to quantify the typical number of grains along the length (L/2a) and across the thickness (t/2c) of a nominal strut. The inset figures show the corresponding grain instantiations, depicted in an undeformed state.

grain along the strut length and more than one grain across the strut thickness, the plateau stress and energy absorption capacity increase approximately linearly with inverse square root of grain size, exhibiting characteristic Hall-Petch-like behavior. These findings are consistent with experimental observations by Goussery et al. [28] for open-cell, non-oxidized, hollow-strut nickel foams. They found through experimental observation that the open-cell nickel foams exhibited Hall-Petch strengthening behavior as long as the grain size was smaller than the strut-wall thickness; as grain size increased and became less "bamboo-like", the yield strength of the foams saturated.

Based on the results presented in Section 3, it is evident that the extent to which grain structure impacts the crushing behavior of the open-cell foam depends on the surface conditions. For a given grain size, the oxidized foam is generally stronger than the non-oxidized foam, owing to the oxidation layer that serves as a barrier to dislocation motion at the free surfaces of the struts. However, as evident from the stress-strain curves in Figs. 8 and 9 and the Hall-Petch-like responses of $\sigma_{plateau}$ and U depicted in Figs. 10 and 11, the grain size has a much more pronounced effect on the mechanical response of the non-oxidized foam than on that of the oxidized foam. The experimental evidence presented by Goussery et al. [28] supports the assertion that "dislocation loops can easily escape across free surfaces" of non-oxidized foams once grain size becomes equal to the strut-wall thickness. Recall that works by Crone et al. [48] and Lee et al. [30] also suggest a reduction in barrier to dislocation motion near free surfaces. This phenomenon is modeled in the current work as a free-surface softening mechanism for non-oxidized
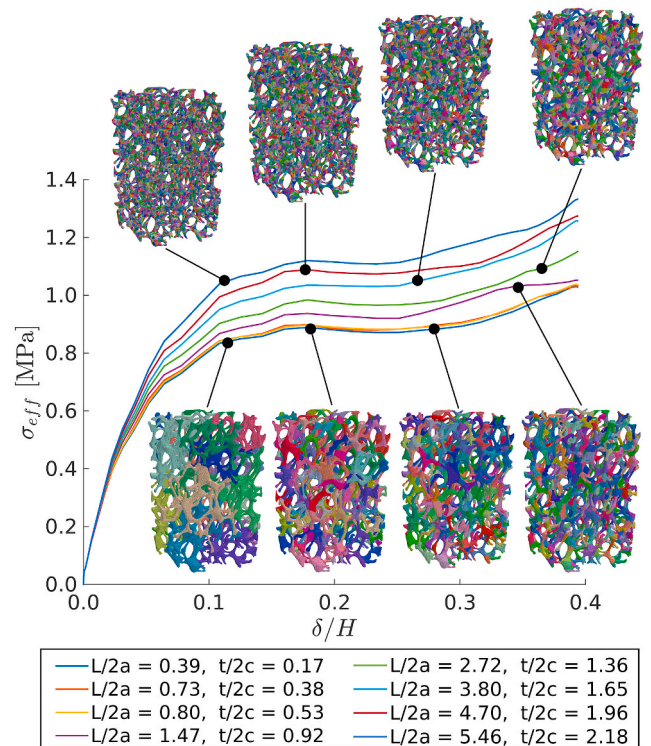

Fig. 9. Effective stress-strain responses of different grain-resolved, **oxidized** foam models. The average grain size is normalized by average geometric parameters of the struts to quantify the number of grains along the length (L/2a) and across the thickness (t/2c) of a nominal strut. The inset figures show the corresponding grain instantiations, depicted in an undeformed state.
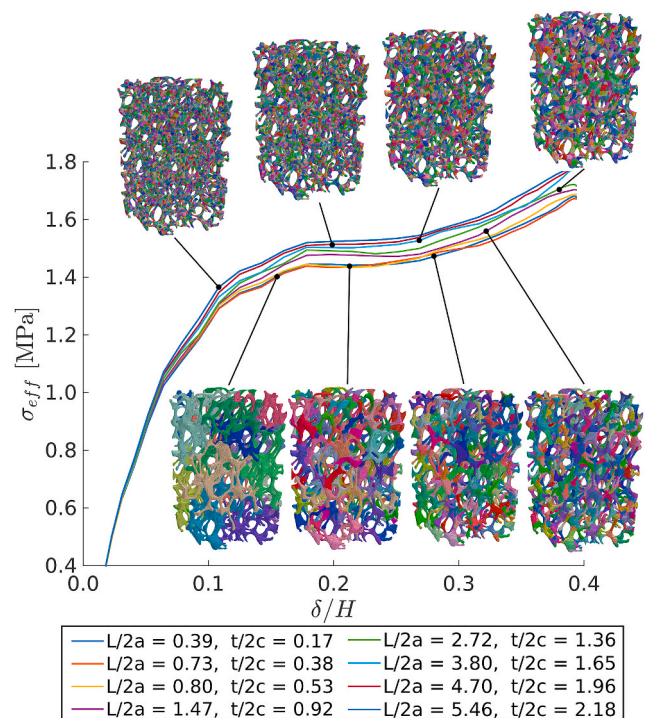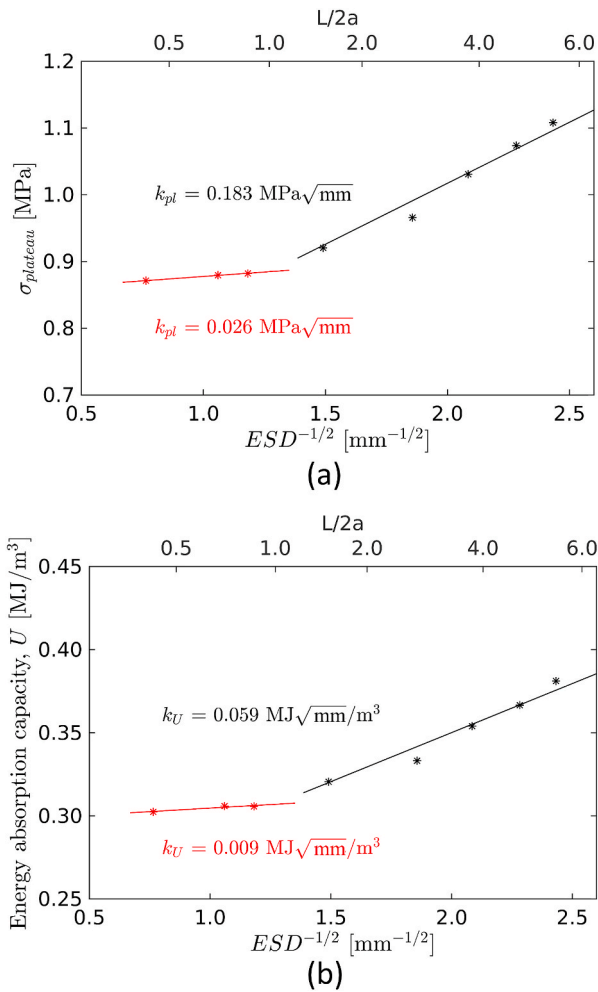
Fig. 10. Compressive properties for **non-oxidized**, Al-6101-T6 foam models: (a) plateau stress, $\sigma_{plateau}$, and (b) energy absorption capacity, U.
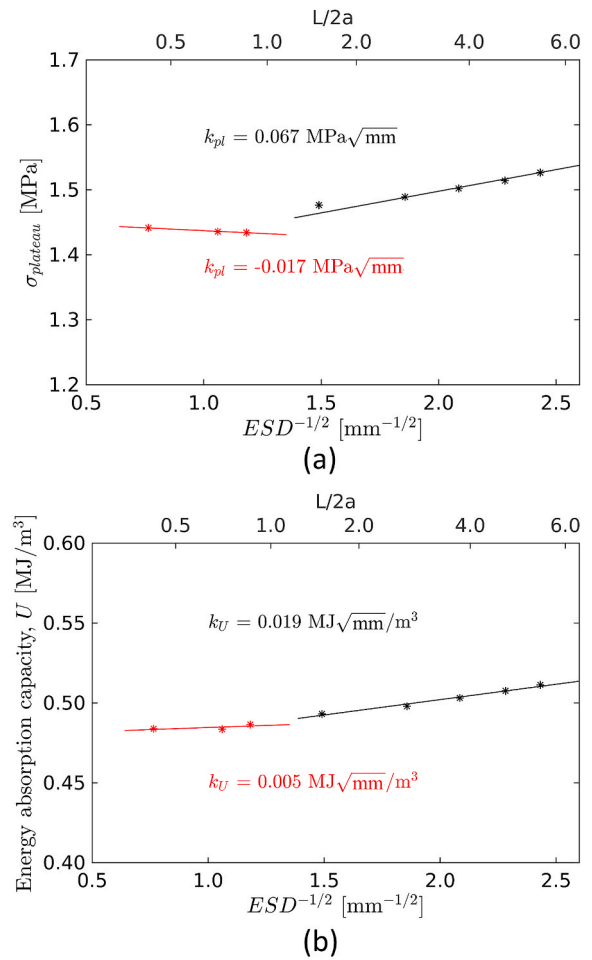

Fig. 11. Compressive properties for **oxidized**, Al-6101-T6 foam models: (a) plateau stress, $\sigma_{plateau}$, and (b) energy absorption capacity, U.

foams, described in Section 2.3. In the presence of an oxidation layer, however, the free surfaces are implicitly modeled as barriers to dislocation motion (analogous to grain boundaries). Based on the findings from this work, with corroboration from the available literature, it is asserted that the ratio of non-oxidized free-surface area to grain-boundary area dictates the variability in mechanical response of open-cell metallic foams. In other words, the range of crush response is smaller for the oxidized foams than for the non-oxidized foams studied herein because the lack of unconstrained surface area on the strut boundaries of the oxidized foam effectively bounds the range of dislocation-barrier spacing and, in turn, bounds the overall mechanical response.

In summary, the geometrical constraint of the struts, in tandem with the constraint imposed due to surface conditions, plays a critical role in governing the effect of grain size on crushing response of open-cell metallic foams.

4.2. Comparison of CPFEM results to the Gibson-Ashby model

The Gibson-Ashby model [1,55] is a well-known closed-form expression that relates the plastic collapse strength of an open-cell foam (σ_{pl}^*) to the yield strength of the fully dense material (σ_y), as follows:

$$\frac{\sigma_{pl}^*}{\sigma_y} = C_4(\rho_r)^{3/2}, \tag{13}$$

where ρ_r is the relative density of the foam, and C_4 is a constant that can

be determined by fitting to experimental data and is, therefore, considered to be empirical. For example, Ashby et al. [1] tested both open-cell metal foams and closed-cell polymer foams and plotted the normalized strength versus relative density. The experimental results were well fitted using Eqn. (13) with a constant C_4 of 0.3. Zhou et al. [24] utilized a four-strut unit cell extracted from Duocel® open-cell aluminum foams to estimate the lower and upper bounds of the foam strengths. The results gave minimum and maximum values of C_4 of 0.34 and 0.44, respectively. The work of Andrews et al. [56] determined the value of C_4 to span between 0.25 and 0.35 for most open-cell metal foams. These cases demonstrate that for open-cell metallic foam (typically with relative density of 30% or lower), the Gibson-Ashby scaling relationship is able to accurately predict the plastic collapse strength provided C_4 is appropriately defined.

We now compare the results obtained using the high-fidelity numerical simulations with strength predictions using the Gibson-Ashby formula. The relative density of the foam, ρ_r, is found to be 6.81%,[2] which is within the range of the manufacturer-reported values for the sample. For both the non-oxidized and oxidized foams, the Gibson-Ashby formula is evaluated three different ways. First, we evaluate Eqn. (13) according to common practice, viz., by using a value of σ_y for the base material taken from a user handbook or similar reference (193 MPa for aluminum 6101-T6 [57]) and a commonly accepted value of C_4 (0.3). Second, C_4 is again assumed to be 0.3; however, a

---

[2] Relative density is calculated by dividing the voxel count of the foam by the voxel count of the nominal cylindrical volume of the sample.

grain-size-dependent value of σ_y is estimated for the fully dense alloy according to the well-established Hall-Petch relationship. In this case, distinct values of σ_y are estimated using Eqn. (9) based on the average grain sizes (ESD) listed in Fig. 5. A similar approach was recently implemented by Wang et al. [51]. Third, the Gibson-Ashby formula is evaluated using the Hall-Petch-modified value of σ_y, as before, but with a distinct value of C_4 that depends on both surface condition and grain size, described in detail next.

The constant C_4 is investigated to determine its dependence on both grain size (relative to ligament size) and surface condition. To do this, C_4 is inversely determined using the plateau stress from numerical simulation and the Hall-Petch-modified yield strength value from Eqn. (9). For the oxidized foam, C_4 is found to have a constant value of approximately 0.47 across all eight foam instantiations. For the non-oxidized foam, C_4 is found to have a constant value of approximately 0.29 for relatively large grain sizes (ESD of 716 μm or larger) and to increase linearly with decreasing grain size otherwise, which is consistent with the saturation trends discussed above. By normalizing the expression of grain size with respect to nominal strut thickness ($t = 270$ μm, see subsection 3.2), the relationship between C_4 and grain size for non-oxidized foam can be expressed using the following conditional equation[3]:

$$C_4 = \begin{cases} 0.29, & \text{if } t/ESD < 0.5 \\ 0.0508(t/ESD) + 0.2624, & \text{if } t/ESD > 0.5. \end{cases} \quad (14)$$

Thus, the third approach for evaluating the Gibson-Ashby formula incorporates the appropriate value of C_4 based on surface condition (oxidized or non-oxidized) and grain size.

Figs. 12 and 13 present comparisons between the plateau stress derived from high-fidelity numerical simulations and the plastic collapse strength based on the Gibson-Ashby formula, evaluated using the three aforementioned approaches. As shown in both figures, the Gibson-Ashby formula, when evaluated using a constant value of σ_y and a commonly

Fig. 12. Comparison between plateau stress based on high-fidelity numerical simulations and the plastic collapse strength based on the Gibson-Ashby formula versus average grain size for **non-oxidized** open-cell aluminum 6101-T6 foam. The Gibson-Ashby formula is evaluated using three different approaches for estimating σ_y and C_4. Grain size is based on equivalent spherical diameter (ESD).

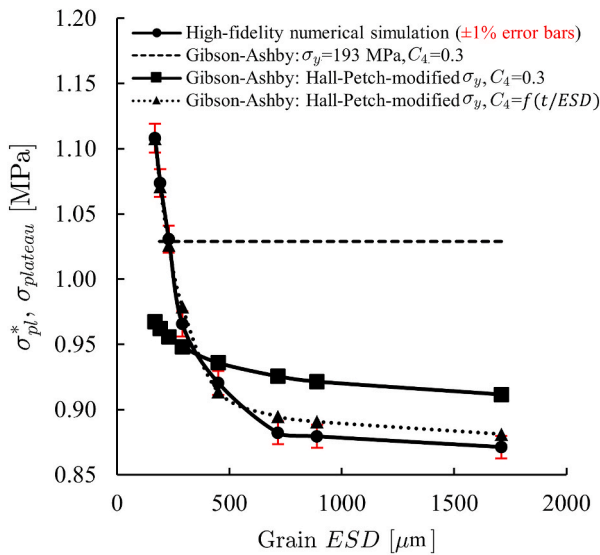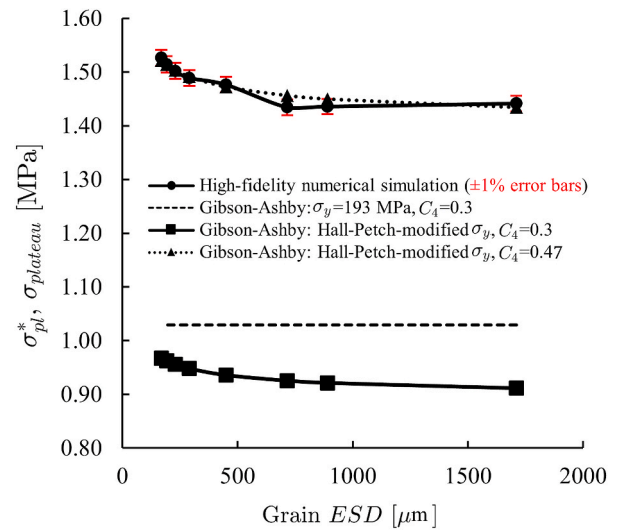[3] See Fig. 14 in the Appendix for goodness of fit.

Fig. 13. Comparison between plateau stress based on high-fidelity numerical simulations and the plastic collapse strength based on the Gibson-Ashby formula versus average grain size for **oxidized** open-cell aluminum 6101-T6 foam. The Gibson-Ashby formula is evaluated using three different approaches for estimating σ_y and C_4. Grain size is based on equivalent spherical diameter (ESD).

accepted value of 0.3 for C_4, provides an estimate of plastic collapse strength that is independent of both surface condition and grain size. For the non-oxidized surface condition, this estimate appears to be accurate for a very narrow range of grain size (approximately 250 μm for the foam analyzed here). For the oxidized surface condition, the plateau stress is significantly underpredicted by using this approach. By modifying σ_y to incorporate Hall-Petch effects of the fully dense material (while maintaining a value of 0.3 for C_4), the shape of the plastic-collapse curves in Figs. 12 and 13 better represent the expected behavior of the foams for both surface conditions compared to the first approach. However, plateau stress is still significantly underpredicted for the oxidized foam. Finally, by updating both σ_y and C_4 to account for surface condition and grain-size effects, the approximation of plastic collapse strength using the Gibson-Ashby formula falls within 1% of the expected values from the high-fidelity numerical simulations. The fact that a relatively high and constant value of C_4 (0.47) is able to capture the plateau stress of the oxidized foam across all grain sizes is indicative of the strengthening effect that the oxidation layer has on the range of mechanical response of the foam, as discussed above in Section 4.1. On the other hand, in the absence of an oxidation layer, C_4 exhibits a strong dependence on grain size (beyond a specific grain-size threshold).

In summary, the results from this study suggest that by estimating σ_y for the fully dense alloy using a Hall-Petch approximation, and by updating C_4 to account for anticipated surface conditions (and, in the case of non-oxidized foam, to further account for effect of grain size with respect to strut thickness, according to Eqn. (14)), the Gibson-Ashby formula can be dramatically improved and generalized.

4.3. Limitations, implications, and scope of future work

The high-fidelity numerical framework presented above provides a way of systematically controlling grain structure to investigate its effect on mechanical response of open-cell foams, a task that would otherwise be difficult or impossible to achieve experimentally. Furthermore, the framework is general enough that it could be applied to investigate additive-manufactured metal lattice structures, a rapidly growing area of interest. Nonetheless, there are a number of limitations associated with the current modeling framework that merit further discussion.

One limitation of the simulations described herein is that hardening

is neglected within the constitutive model. As mentioned in Section 2.2, this assumption is justified for the reasons that (1) localized hardening likely has a negligible effect on the bulk (homogenized) response of the foam compared to other structural mechanisms, like cell collapse; and (2) lack of mechanical test data for grain-resolved samples of foam precludes the ability to perform a more refined model calibration than that reported in Section 2.4. Based on the stress-strain results presented in this study, it is shown that the numerical framework, even by neglecting slip-system-level hardening, is capable of reproducing bulk crush behavior that is characteristic of cellular metals. Future work could investigate the effect of incorporating slip-system-level hardening into the constitutive model.

Another limitation of the current work is that, in an effort to isolate effects of grain size and surface condition, only one foam density was examined. Recall that X-ray CT data from one sample of 40 ppi 6.81% dense foam was used to instantiate different grain-resolved foam models. To the extent possible, we have attempted to normalize the descriptions of the foam in this work to help generalize the findings (e.g., by expressing grain size with respect to nominal ligament size). However, it is unknown whether the findings pertaining to effect of grain size and surface condition on crushing response are applicable across a broad range of foam densities. Thus, using a similar approach to that presented here, future work could investigate the combined influence of foam density and grain structure on mechanical response of open-cell foams.

Finally, the results presented herein should be experimentally validated, which remains an active area of research by the authors. Unlike for fully dense volumes of material, 3D experimental characterization of ultra-low-density open-cell foams at the crystalline level presents unique challenges due to the sparse and fragile network of struts, and these challenges have only recently begun to be addressed [27]. Whereas, X-ray CT has become a relatively common approach for characterizing the 3D morphology of cellular and lattice-like structures, characterizing grain structure involves diffraction techniques that require sophisticated sample preparation (e.g., mounting the foam in epoxy and polishing to perform electron backscatter diffraction, as done in Ref. [58]) or access to 3D grain-mapping techniques that are limited in availability, as described by Plumb et al. [27]. In the absence of experimental data that would otherwise enable direct comparison to experiment, we have attempted in this work to compare our simulation results to the (limited) observations in literature that report grain-scale measurements of open-cell metallic foams. Future work should continue to focus on generating experimental data for further validation.

It is worth highlighting that very recently, researchers have demonstrated the capability of adaptively refining the grain structure in open-cell Mg foam using a multi-axial forging process [51]. The capability to experimentally control grain size implies that findings based on high-fidelity numerical simulations could be used to guide or inform the actual manufacturing process. Therefore, there is a significant opportunity moving forward to link the structure-property predictions from this work with process-structure capabilities to fully exploit process-structure-property relationships, thus enabling design optimization of open-cell metallic foams and lattice structures.

5. Conclusions

This work investigates the coupled effects of surface conditions and grain structure on the bulk mechanical response of investment-cast, open-cell aluminum foam using high-fidelity numerical simulations. Grain structure is systematically varied and overlaid on a foam geometry derived from X-ray computed tomography to create multiple instantiations of the foam with explicitly resolved grain structure. The numerical simulations incorporate a crystal-plasticity constitutive model to capture the grain-to-continuum mechanical response of the foam. Grain-boundary strengthening and free-surface softening mechanisms are implemented to account for, respectively, the Hall-Petch effect

in polycrystalline materials and the effect of unconstrained slip-based deformation associated with the high specific surface area inherent to open-cell foams and lattice structures. The constitutive model is calibrated using force-displacement data from an experimental crush test of the foam sample on which the above-mentioned X-ray computed tomography measurements are based. From the results of this numerical investigation, the following conclusions are drawn:

1. Consistent with experimental observations from the literature, the plateau stress and energy absorption capacity of the foam exhibit Hall-Petch-like behavior for grain sizes below a certain threshold, above which the mechanical behavior of the bulk foam tends to saturate. For the aluminum 6101-T6 foam investigated here, the threshold for saturation occurs when there is nominally less than one complete grain along the strut length (i.e., when, on average, the grains extend beyond the length of the struts) and approximately one grain through the strut thickness.
2. For a given grain structure, the plateau stress is greater in the oxidized foam than in the non-oxidized foam, owing to the strengthening effect of the oxidation layer, which serves as a barrier to dislocation motion.
3. The extent to which grain structure impacts the crushing behavior of open-cell foam depends on the surface conditions. The effect of grain size on mechanical response is more pronounced in the non-oxidized case than in the oxidized case, suggesting that the ratio of unconstrained free-surface area to grain-boundary area controls the range of variability in mechanical response of open-cell metallic foams.
4. While conventional evaluation of the Gibson-Ashby model is incapable of accounting for effect of grain size and surface condition on the plastic collapse strength of open-cell metallic foam, modifying the values of σ_y and C_4 in the model to account for grain size and surface condition is shown to enhance both the accuracy and generalizability of the Gibson-Ashby model. Surface- and grain-size-dependent estimates of C_4 are provided based on results from the high-fidelity numerical simulations.

Data availability

The raw/processed data required to reproduce these findings cannot be shared at this time as the data also forms part of an ongoing study.

CRediT authorship contribution statement

Dongfang Zhao: Methodology, Software, Formal analysis, Investigation, Writing – original draft, Writing – review & editing, Visualization. **Kristoffer E. Matheson:** Investigation. **Brian R. Phung:** Software. **Steve Petruzza:** Software, Investigation, Writing – original draft. **Michael W. Czabaj:** Resources, Writing – review & editing, Project administration. **Ashley D. Spear:** Conceptualization, Methodology, Resources, Writing – original draft, Writing – review & editing, Supervision, Project administration, Funding acquisition.

Declaration of competing interest

The authors declare that they have no known competing financial interests or personal relationships that could have appeared to influence the work reported in this paper.
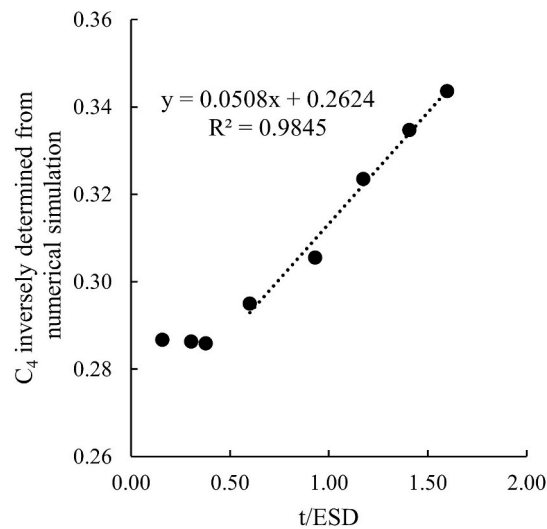
Acknowledgements

Appendix

Fig. 14. Relationship between C_4 in the Gibson-Ashby model and the nominal ligament thickness normalized by grain size (t/ESD). Values of C_4 are inversely determined using the plateau stress from high-fidelity numerical simulation.

References

[1] M.F. Ashby, R.M. Medalist, The mechanical properties of cellular solids, Metall. Trans. A 14 (9) (1983) 1755–1769.

[2] A.G. Evans, J. Hutchinson, M. Ashby, Multifunctionality of cellular metal systems, Prog. Mater. Sci. 43 (3) (1998) 171–221.

[3] J. Banhart, Manufacture, characterisation and application of cellular metals and metal foams, Prog. Mater. Sci. 46 (6) (2001) 559–632.

[4] J. Banhart, Aluminum foams: on the road to real applications, MRS Bull. 28 (4) (2003) 290–295.

[5] C. Zhao, W. Lu, Y. Tian, Heat transfer enhancement for thermal energy storage using metal foams embedded within phase change materials (pcms), Sol. Energy 84 (8) (2010) 1402–1412.

[6] R. Singh, P. Lee, R. Dashwood, T. Lindley, Titanium foams for biomedical applications: a review, Mater. Technol. 25 (3–4) (2010) 127–136.

[7] L.E. Murr, S. Gaytan, F. Medina, H. Lopez, E. Martinez, B. Machado, D. Hernandez, L. Martinez, M. Lopez, R. Wicker, et al., Next-generation biomedical implants using additive manufacturing of complex, cellular and functional mesh arrays, Phil. Trans. Math. Phys. Eng. Sci. 368 (1917) (2010) 1999–2032.

[8] L.E. Murr, S.M. Gaytan, E. Martinez, F. Medina, R.B. Wicker, Next generation orthopaedic implants by additive manufacturing using electron beam melting, Int. J. Biomater. (2012).

[9] W.-Y. Jang, S. Kyriakides, On the crushing of aluminum open-cell foams: Part i. experiments, Int. J. Solid Struct. 46 (3–4) (2009) 617–634.

[10] P. Schüler, S.F. Fischer, A. Bührig-Polaczek, C. Fleck, Deformation and failure behaviour of open cell al foams under quasistatic and impact loading, Mater. Sci. Eng., A 587 (2013) 250–261.

[11] M. Kader, M. Islam, M. Saadatfar, P. Hazell, A. Brown, S. Ahmed, J. Escobedo, Macro and micro collapse mechanisms of closed-cell aluminium foams during quasi-static compression, Mater. Des. 118 (2017) 11–21.

[12] A. Kaya, C. Fleck, Deformation behavior of open-cell stainless steel foams, Mater. Sci. Eng., A 615 (2014) 447–456.

[13] J. Zhou, W. Soboyejo, Compression–compression fatigue of open cell aluminum foams: macro-/micro-mechanisms and the effects of heat treatment, Mater. Sci. Eng., A 369 (1–2) (2004) 23–35.

[14] L. Gong, S. Kyriakides, W.-Y. Jang, Compressive response of open-cell foams. part i: morphology and elastic properties, Int. J. Solid Struct. 42 (5–6) (2005) 1355–1379.

[15] S. Gaitanaros, S. Kyriakides, A.M. Kraynik, On the crushing response of random open-cell foams, Int. J. Solid Struct. 49 (19–20) (2012) 2733–2743.

[16] S. Kashef, A. Asgari, T.B. Hilditch, W. Yan, V.K. Goel, P. Quadbeck, P.D. Hodgson, Fracture mechanics of stainless steel foams, Mater. Sci. Eng., A 578 (2013) 115–124.

[17] W.-Y. Jang, S. Kyriakides, On the crushing of aluminum open-cell foams: Part ii analysis, Int. J. Solid Struct. 46 (3–4) (2009) 635–650.

[18] L. Gong, S. Kyriakides, Compressive response of open cell foams part ii: initiation and evolution of crushing, Int. J. Solid Struct. 42 (5–6) (2005) 1381–1399.

[19] Y. Hangai, R. Yamaguchi, S. Takahashi, T. Utsunomiya, O. Kuwazuru, N. Yoshikawa, Deformation behavior estimation of aluminum foam by x-ray ct image-based finite element analysis, Metall. Mater. Trans. 44 (4) (2013) 1880–1886.

[20] S. Bardenhagen, A. Brydon, J. Guilkey, Insight into the physics of foam densification via numerical simulation, J. Mech. Phys. Solid. 53 (3) (2005) 597–617.

[21] A. Brydon, S. Bardenhagen, E. Miller, G. Seidler, Simulation of the densification of real open-celled foam microstructures, J. Mech. Phys. Solid. 53 (12) (2005) 2638–2660.

[22] W.-Y. Jang, A.M. Kraynik, S. Kyriakides, On the microstructure of open-cell foams and its effect on elastic properties, Int. J. Solid Struct. 45 (7–8) (2008) 1845–1875.

[23] J. Zhou, S. Allameh, W. Soboyejo, Microscale testing of the strut in open cell aluminum foams, J. Mater. Sci. 40 (2) (2005) 429–439.

[24] J. Zhou, C. Mercer, W. Soboyejo, An investigation of the microstructure and strength of open-cell 6101 aluminum foams, Metall. Mater. Trans. 33 (5) (2002) 1413–1427.

[25] E. Amsterdam, P. Onck, J.T.M. De Hosson, Fracture and microstructure of open cell aluminum foam, J. Mater. Sci. 40 (22) (2005) 5813–5819.

[26] A. Jung, S. Luksch, S. Diebels, F. Schäfer, C. Motz, In-situ and ex-situ microtensile testing of individual struts of al foams and ni/al hybrid foams, Mater. Des. 153 (2018) 104–119.

[27] J.C. Plumb, J.F. Lind, J.C. Tucker, R. Kelley, A.D. Spear, Three-dimensional grain mapping of open-cell metallic foam by integrating synthetic data with experimental data from high-energy x-ray diffraction microscopy, Mater. Char. 144 (2018) 448–460.

[28] V. Goussery, Y. Bienvenu, S. Forest, A.-F. Gourgues, C. Colin, J.-D. Bartout, Grain size effects on the mechanical behavior of open-cell nickel foams, Adv. Eng. Mater. 6 (6) (2004) 432–439.

[29] B.V. Krishna, S. Bose, A. Bandyopadhyay, Strength of open-cell 6101 aluminum foams under free and constrained compression, Mater. Sci. Eng., A 452 (2007) 178–188.

[30] K. Lee, J. Lewandowski, Effects of microstructural characteristics on mechanical properties of open-cell nickel foams, Mater. Sci. Technol. 21 (11) (2005) 1355–1358.

[31] J. Zhou, Z. Gao, A. Cuitino, W. Soboyejo, Effects of heat treatment on the compressive deformation behavior of open cell aluminum foams, Mater. Sci. Eng., A 386 (1–2) (2004) 118–128.

[32] D. Lehmhus, J. Banhart, Properties of heat-treated aluminium foams, Mater. Sci. Eng., A 349 (1–2) (2003) 98–110.

[33] M. Mukherjee, U. Ramamurty, F. Garcia-Moreno, J. Banhart, The effect of cooling rate on the structure and properties of closed-cell aluminium foams, Acta Mater. 58 (15) (2010) 5031–5042.

[34] K. Chan, S. Chan, Effect of cell morphology and heat treatment on compressive properties of aluminum foams, Mater. Manuf. Process. 19 (3) (2004) 407–422.

[35] P. Schüler, R. Frank, D. Uebel, S.F. Fischer, A. Bührig-Polaczek, C. Fleck, Influence of heat treatments on the microstructure and mechanical behaviour of open cell alsi7mg0. 3 foams on different lengthscales, Acta Mater. 109 (2016) 32–45.

[36] Z. Wang, Z. Li, J. Ning, L. Zhao, Effect of heat treatments on the crushing behaviour and energy absorbing performance of aluminium alloy foams, Mater. Des. 30 (4) (2009) 977–982.

[37] E. Andrews, G. Gioux, P. Onck, L. Gibson, Size effects in ductile cellular solids. part ii: experimental results, Int. J. Mech. Sci. 43 (3) (2001) 701–713.

[38] M.A. Groeber, M.A. Jackson, Dream. 3d: a digital representation environment for the analysis of microstructure in 3d, Integrating Mater. Manuf. Innovat. 3 (1) (2014) 5.

[39] J.C. Tucker, A.D. Spear, A tool to generate grain-resolved open-cell metal foam models, Integrating Mater. Manuf. Innovat. 8 (2) (2019) 247–256.

[40] M. Smith, ABAQUS/Explicit User's Manual, Simulia, 2009 version 6.9.

[41] K. Matouš, A.M. Maniatty, Multiscale modeling of elasto-viscoplastic polycrystals subjected to finite deformations, Interact. Multiscale Mech. 2 (4) (2009) 375–396.

[42] J. Bozek, J. Hochhalter, M. Veilleux, M. Liu, G. Heber, S. Sintay, A. Rollett, D. Littlewood, A. Maniatty, H. Weiland, et al., A geometric approach to modeling microstructurally small fatigue crack formation: I. probabilistic simulation of constituent particle cracking in aa 7075-t651, Model. Simulat. Mater. Sci. Eng. 16 (6) (2008), 065007.

[43] A.D. Spear, J.D. Hochhalter, A.R. Cerrone, S.F. Li, J.F. Lind, R.M. Suter, A. R. Ingraffea, A method to generate conformal finite-element meshes from 3d measurements of microstructurally small fatigue-crack propagation, Fatig. Fract. Eng. Mater. Struct. 39 (6) (2016) 737–751.

[44] K.D. Pierson, J.D. Hochhalter, A.D. Spear, Data-driven correlation analysis between observed 3d fatigue-crack path and computed fields from high-fidelity, crystal-plasticity, finite-element simulations, JOM 70 (7) (2018) 1159–1167.

[45] R. Leavy, J. Guilkey, B. Phung, A. Spear, R. Brannon, A convected-particle tetrahedron interpolation technique in the material-point method for the mesoscale modeling of ceramics, Comput. Mech. (2019) 1–21.

[46] K. Matouš, A.M. Maniatty, Finite element formulation for modelling large deformations in elasto-viscoplastic polycrystals, Int. J. Numer. Methods Eng. 60 (14) (2004) 2313–2333.

[47] M. Nakai, G. Itoh, The effect of microstructure on mechanical properties of forged 6061 aluminum alloy, Mater. Trans. 55 (1) (2014) 114–119.

[48] J.C. Crone, L.B. Munday, J. Knap, Capturing the effects of free surfaces on void strengthening with dislocation dynamics, Acta Mater. 101 (2015) 40–47.

[49] C.-L. Lee, S. Li, A half-space peierls–nabarro model and the mobility of screw dislocations in a thin film, Acta Mater. 55 (6) (2007) 2149–2157.

[50] R.T. Barrett, Fastener Design Manual, vol. 1228, NASA, Scientific and Technical Information Division, 1990.

[51] Y. Wang, H. Huang, G. Jia, G. Ke, J. Zhang, G. Yuan, Effect of grain size on the mechanical properties of mg foams, J. Mater. Sci. Technol..

[52] J. Ahrens, B. Geveci, C. Law, Paraview: an end-user tool for large data visualization, The visualization handbook 717.

[53] S. Petruzza, A. Gyulassy, S. Leventhal, J.J. Baglino, M. Czabaj, A.D. Spear, V. Pascucci, High-throughput feature extraction for measuring attributes of deforming open-cell foams, IEEE Trans. Visual. Comput. Graph. 26 (1) (2019) 140–150.

[54] A. Gyulassy, P.-T. Bremer, V. Pascucci, Shared-memory parallel computation of morse-smale complexes with improved accuracy, IEEE Trans. Visual. Comput. Graph. 25 (1) (2018) 1183–1192.

[55] L.J. Gibson, M.F. Ashby, Cellular Solids: Structure and Properties, Cambridge university press, 1999.

[56] E. Andrews, W. Sanders, L.J. Gibson, Compressive and tensile behaviour of aluminum foams, Mater. Sci. Eng., A 270 (2) (1999) 113–124.

[57] K. Anderson, J. Weritz, J.G. Kaufman, Asm handbook, volume 2b, properties and selection of aluminum alloys, Elastic 2 (2019), 0–098.

[58] K.E. Matheson, K.K. Cross, M.M. Nowell, A.D. Spear, A multiscale comparison of stochastic open-cell aluminum foam produced via conventional and additive-manufacturing routes, Mater. Sci. Eng., A 707 (2017) 181–192.